



Model Predictive Cooling Control of Cylindrical Battery Cells Through Tab and Surface Channels

Downloaded from: <https://research.chalmers.se>, 2026-04-14 11:54 UTC

Citation for the original published paper (version of record):

Peprah, G., Wik, T., Huang, Y. et al (2025). Model Predictive Cooling Control of Cylindrical Battery Cells Through Tab and Surface Channels. American Control Conference: 4071-4076.
<http://dx.doi.org/10.23919/ACC63710.2025.11107872>

N.B. When citing this work, cite the original published paper.

© 2025 IEEE. Personal use of this material is permitted. Permission from IEEE must be obtained for all other uses, in any current or future media, including reprinting/republishing this material for advertising or promotional purposes, or reuse of any copyrighted component of this work in other works.

Model Predictive Cooling Control of Cylindrical Battery Cells Through Tab and Surface Channels

Godwin K. Peprah, Torsten Wik, Yicun Huang, Faisal Altaf, Changfu Zou

Abstract—Tab cooling offers more uniform cooling across the battery, while surface cooling is more effective at removing heat due to a larger cooling contact area. This work formalises the optimal integration of tab and surface cooling methods to leverage their unique strengths. This optimal integration control problem is addressed using the Model Predictive Control (MPC) framework, which optimally distributes coolant between the tabs and surfaces of the cylindrical cell to minimise thermal gradients and average temperature rise. The proposed MPC scheme, which includes an advanced thermal model containing the cooling system’s switching mechanism is evaluated against conventional side-only and base-only electric vehicle battery cooling schemes, under the urban dynamometer driving schedule. Results demonstrate significant thermal performance improvements of the proposed MPC scheme over the conventional cooling methods.

I. INTRODUCTION

Lithium (Li)-ion batteries have remained a preferred choice of energy storage for numerous applications, including electric vehicles (EVs), portable electronics and renewable energy storage systems, due to their extended cycle life, high energy and power density in comparison to other secondary batteries [1]. However, their performance, lifespan, and safety can be significantly compromised by thermal issues such as overheating and thermal runaway [2]. Consequently, effective thermal management of Li-ion batteries has become a pressing concern, driving research efforts to address thermal-related challenges.

Previous literature studies have investigated different cooling strategies, including the effect of tab (electrical terminals) cooling and cell surface cooling, on battery thermal performance. Bolsinger *et al.* and Li *et al.* demonstrated in [3,4] that tab cooling, despite utilizing only about 5% of the total cell surface area, resulted in a reduction of internal temperature inhomogeneities compared to surface cooling in cylindrical Li-ion cells. Surface cooling, which makes use of about 60% of the total cell surface, was less effective in reducing inhomogeneities but can maintain the cell at a lower average temperature. Thus, surface and tab cooling each possesses distinct advantages and limitations. However,

This work was funded in part by the Swedish Electromobility Centre and the Swedish Energy Agency under grant No. 13011 and in part by the Swedish Research Council under grant No. 2019-04873.

G. K. Peprah, T. Wik, Y. Huang, and C. Zou are with the Department of Electrical Engineering, Chalmers University of Technology, 41296 Gothenburg, Sweden. (Emails: godwinp@chalmers.se; tw@chalmers.se; yicun@chalmers.se; changfu.zou@chalmers.se).

F. Altaf is with the Department of Electromobility, Volvo Group Trucks Technology, 40508 Gothenburg, Sweden. (Email: faisal.altaf@volvo.com).

to the best of our knowledge, the state-of-the-art literature lacks a battery control framework that systemically explores the optimal combination of these two cooling methods for advanced battery temperature management.

This work formalises the integration of the two cooling strategies as an optimal control problem. The goal is to optimally split the coolant flow between the tabs and surface of the cell to minimise both the average temperature rise and the thermal gradients within the battery cell, regardless of operating conditions. The problem is solved in a receding horizon fashion using the model predictive control (MPC) framework, which also guarantees constraints to be satisfied.

In the MPC framework, we adopt a thermal model developed in our previous work [5,6] as the predictive model. This model, based on the Chebyshev Spectral-Galerkin (CSG) method [7] and model component decomposition, is computationally efficient and accurately captures the two-dimensional (2D) temperature distribution within battery cells. It also allows independent control of the tab and surface cooling channels, making it particularly well-suited for solving the real-time optimal control problem of coolant flow distribution to the tabs and surface of the battery cell. To obtain insights into how the coolant flow is controlled, we incorporate a switching mechanism of the valves that distribute coolant to the different sides of the cell into the CSG model. The switching operation can respond dynamically to changing thermal conditions and operational requirements. Integrating this aspect into the thermal model allows the evaluation of the system’s dynamic response to temperature fluctuations.

II. CONTROL SCHEME OVERVIEW

A. Reference control architecture

Fig. 1 shows an EV battery thermal management system (BTMS). It comprises a coolant circulation system, where a mixture of water and glycol, driven by a pump, flows through channels embedded within the high-voltage battery pack. Cooling plates, either attached to the curved surface or the base of battery cells, facilitate heat absorption and removal. The heat absorbed by the coolant is then transferred to a heat exchanger, which dissipates it to the ambient air or a secondary cooling circuit, such as a heat pump, depicted in the green-dashed box in Fig. 1.

Our proposed optimal coolant-split control strategy can be realised by the active cooling architecture shown in the red-dashed box of Fig. 1. This distinctive architecture known in

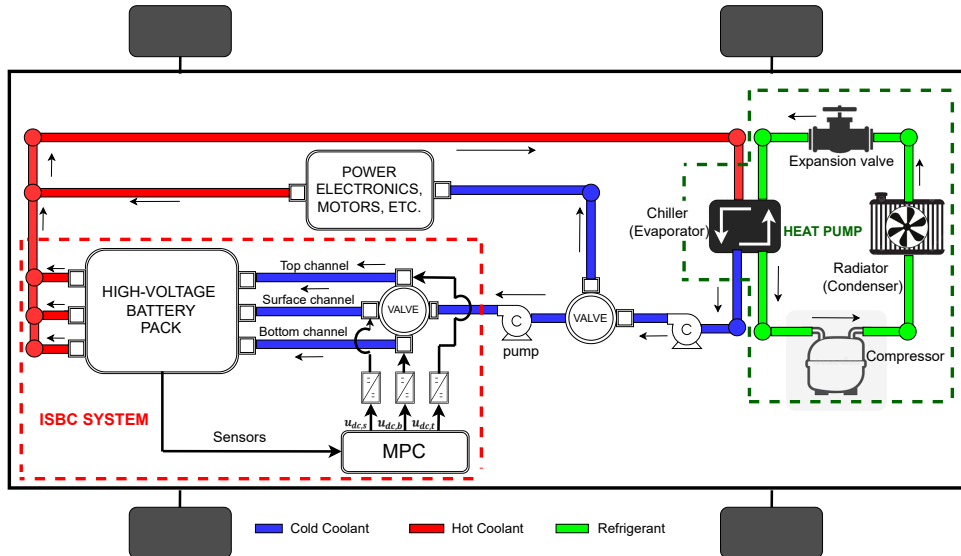


Fig. 1: Battery thermal management system of an EV consisting of a heat pump with its refrigeration cycle (green-dashed box) and the proposed integrated switched battery cooling (ISBC) system (red-dashed box). Centrifugal pumps drive the water and glycol mixture through the coolant circulation system. The red-coloured channels represent the hot coolant, the blue, the cooled coolant, and the green, the refrigerant. It is assumed that the control of the chiller manages to attenuate temperature variations in the return flow from the batteries.

this work as the Integrated Switched Battery Cooling (ISBC) system, requires three separate cooling channels, each targeting different parts of the cell; the curved surface, top, and bottom sides. For simplicity, we assume the coolant flows to the batteries instantaneously, without any input delay. Coolant flow is regulated by a three-way solenoid valve [8,9], actuated by direct current (DC)-DC power converters, which splits the flow among the three channels. To achieve the desired thermal performance objectives, the MPC controller generates modulating signals $u_{dc,\varphi}(t) \in [0, 1]$, where the subscript $\varphi \in \{s, t, b\}$, with s , t , and b denoting the surface, top, and bottom channels, respectively. Subsequently, these modulating signals are fed into a pulse width modulator (PWM), which produces binary switching functions $s_\varphi(t) \in \{0, 1\}$ to activate transistors within each power converter. From a control viewpoint, the variables, $u_{dc,\varphi} \in \mathcal{U} \subseteq \mathcal{R}^n$, can be viewed as valve control knobs that determine the degree to which each valve is opened, thus regulating the coolant distribution across the channels.

B. Problem statement

The problem of integrating the tabs and surface cooling methods can be formally defined as follows.

The optimal coolant split control problem (OCSP), is to determine, on the future time interval $[k, k + \tau]$, the coolant flow through the tabs and surface cooling channels that minimises both the temperature gradient and average temperature rise of the battery cell, without violating the physical limits, i.e., battery temperature, valves and converter actuation.

To solve the *OCSP*, we propose a feedback control strategy implemented through an MPC controller. This strategy is illustrated in Fig. 2 for a single cell in the battery pack. The figure provides a detailed view of the ISBC system, including the three cooling channels with their respective valves, PWM and converters. Additionally, a state estimation block is included to provide real-time estimates of unmeasurable temperature quantities. Using these real-time data, the controller continuously adjusts the coolant flows through the cooling channels to ensure that the thermal performance objectives are met, regardless of operating conditions.

Addressing the *OCSP* requires establishing an MPC framework with all its essential components, including a detailed battery thermal model, state estimator, well-defined cost function and constraints. The forthcoming sections outline these MPC components, starting with the predictive model.

III. MODELLING

In this section, we revisit the 2D thermal model for the cylindrical Li-ion cell developed in our previous work [5,6], incorporating the switching mechanism of the converters that control the three-way valve.

A. State Space thermal model

As detailed in [5,6], the control-oriented 2D thermal model for cylindrical battery cells is of the form

$$G\dot{X}(t) = AX(t) + Bu(t) + Fw(t), \quad (1a)$$

$$Y(t) = CX(t) + \hat{T}_p(t), \quad (1b)$$

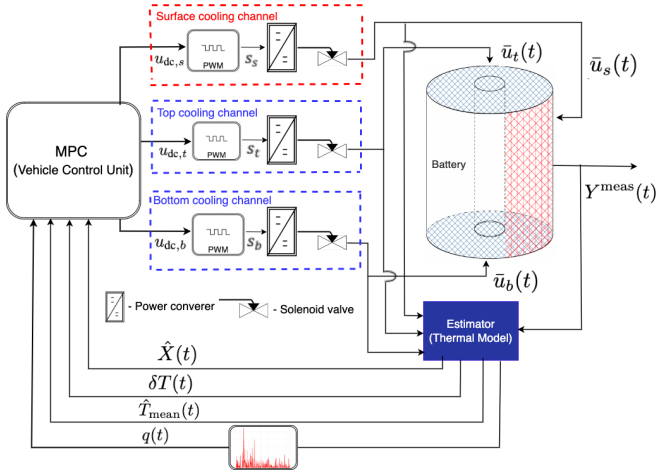


Fig. 2: Feedback control strategy for solving the optimal coolant split control problem *OCSP* using the proposed ISBC system for a single battery cell. The system comprises an MPC controller, temperature sensors, a state estimation block, and three cooling channels for the cell’s tabs and surface, each controlled by a valve-switching mechanism. The tabs fully cover the top and bottom areas of the cell, with their corresponding cooling channels shaded in blue. The surface cooling channel, shaded in red, covers the lateral side of the cell.

where the system matrices G , A , B , C , and vectors X , F , Y , and \hat{T}_p are defined in [5,6]. Equation (1) features the cell boundary conditions in the control vector u as

$$\text{where } u(t) = [u_s(t) \quad u_t(t) \quad u_b(t)]^T, \quad (2)$$

$$u_s(t) = h_s(t)T_{s,\infty}(t), \quad u_t(t) = h_t(t)T_{t,\infty}(t), \quad (3)$$

$$u_b(t) = -h_b(t)T_{b,\infty}(t),$$

are the cooling power applied at the surface, top and bottom sides of the cell, respectively. Here, h and T_∞ denote the convection coefficients and fluid free-stream temperatures, respectively. The disturbance w represents the heat generation rate, $q(t)$.

B. Thermal model with switching mechanism

In this study, we assume that half-bridge DC-DC power converters control the valves. Fig. 3 illustrates the topology of the converter, which consists of two ideal (instantaneous and lossless switching assumed) electronic transistors, with states denoted by $(s_{\varphi,1}, \text{ and } s_{\varphi,2}) \in \{0,1\}$. The transistors are operated by PWM switching functions s_φ . To avoid short-circuiting, $s_{\varphi,1}$ and $s_{\varphi,2}$ are assumed to be orthogonal. Namely, there exists

$$\int_{t-T_{sp}}^t s_{\varphi,1}(\tau)s_{\varphi,2}(\tau)d\tau = 0, \quad (4)$$

where t is time and T_{sp} is the switching period of transistors $s_{\varphi,1}$ and $s_{\varphi,2}$. This orthogonality condition essentially implies that the two transistors cannot be ON simultaneously or overlap.

We intend to control the average behaviour of the ISBC during the switching period T_{sp} using the switching period average framework [10]. This framework enables us to define control actions over the switching period $[t - T_{sp}, t]$, using the duty cycle

$$u_{dc,\varphi}(t) := \frac{1}{T_{sp}} \int_{t-T_{sp}}^t s_\varphi(\tau)d\tau = \frac{s_{\varphi,ON}(t)}{T_{sp}}, \quad (5)$$

where $s_{\varphi,ON}$ is the duration for which s_φ is ON during the switching period. The control signals in (3) are related to $u_{dc,\varphi}$ in (5) through the linear expressions

$$\bar{u}_s(t) = u_s(t)u_{dc,s}, \quad \bar{u}_t(t) = u_t(t)u_{dc,t}, \quad \bar{u}_b(t) = u_b(t)u_{dc,b}, \quad (6)$$

where \bar{u} represents the switched average cooling power for each channel. Replacing the control vector in (2) with the duty-cycle modulated control signals in (6) results in the switched control vector

$$\bar{u}(t) = [\bar{u}_s(t) \quad \bar{u}_t(t) \quad \bar{u}_b(t)]^T. \quad (7)$$

With this, the thermal model of the cylindrical cell, where the control inputs are now functions of the duty cycles for each cooling channel, is established.

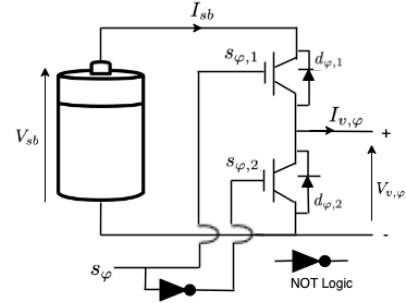


Fig. 3: A simplified schematic of a half-bridge DC-DC power converter. It consists of the switching function s_φ , transistor switches $s_{\varphi,1}$ and $s_{\varphi,2}$, each with diodes $d_{\varphi,1}$ and $d_{\varphi,2}$ in antiparallel. The switching system is powered by a voltage source V_{sb} from a supply battery, with I_{sb} representing the supply battery current. The load current and voltage for the valve are denoted as $I_{v,\varphi}$ and $V_{v,\varphi}$, respectively.

IV. MPC COMPONENTS

A. State estimation

In the cylindrical cell, the core temperature, often the hottest part of the cell is typically not measured by sensors. It is necessary to continuously monitor the core temperature to mitigate irreversible ageing and thermal runaway in a timely fashion. Equations (1)–(3), and (5)–(7) allow the construction of the state observer

$$\dot{\hat{X}}(t) = \bar{A}\hat{X}(t) + \bar{B}\bar{u}(t) + \bar{F}w(t) + K[Y(t) - C\hat{X}(t) - \hat{T}_p(t)], \quad (8)$$

where \hat{X} represent the reconstructed states, including the core temperature, and $\bar{A} = G^{-1}A$, $\bar{B} = G^{-1}B$, and $\bar{F} = G^{-1}F$, with G being invertible. K is the observer gain. Defining the state estimation error $\tilde{X}(t) = \hat{X}(t) - X(t)$, the error dynamics can be found as

$$\dot{\tilde{X}}(t) = (\bar{A} - KC)\tilde{X}(t). \quad (9)$$

Invoking the Kalman rank observability test [11] to (1)–(3), and (5)–(7) shows that the system (\bar{A}, C) is observable. Thus, the eigenvalues of the error dynamics $(\bar{A} - KC)$ can be arbitrarily assigned to be purely stable, guaranteeing that $\tilde{X} \rightarrow 0$ as $t \rightarrow \infty$. For brevity, state estimation is not further elaborated in the present work, and we assume direct access to the state X in the MPC implementation.

B. MPC formulation

The proposed objective function to solve the *OCSP* at time step k is defined as

$$J = \min_{\bar{u}} \sum_{i=0}^{N-1} \left[g_1 \|\bar{T}(k+i)\|_{Q_m}^2 + g_2 \|\delta T(k+i)\|_{Q_\delta}^2 + g_3 \|\Delta u_{dc,\varphi}(k+i)\|_R^2 \right], \quad (10)$$

where N is the prediction horizon and $\|x\|_D^2 := x^T D x$ denotes the weighted norm of vector x , $\{g_i \geq 0; i = 1, \dots, 3\}$ are trade-off weights, tuned to reflect the relative significance of each objective. The first term on the right-hand side of (10)

$$\bar{T}(k+i) = \frac{1}{n} \sum_{j=1}^n T_j(k+i), \quad (11)$$

is the average cell temperature, weighted by a semi-positive definite matrix, Q_m . T_j is the cell temperature at each discrete point j , with n being the total number of points in the cell. Minimising \bar{T} keeps the cell within an optimal temperature range, which is essential for extending its overall lifetime. The second term, $\delta T(k+i)$, represents the thermal gradients within the cell, defined as the spatial derivative of the temperature with respect to the radial r , and axial z , directions of the cell

$$\delta T(k+i) = \frac{d(T_j(k+i))}{d\gamma}, \quad \text{where } \gamma \in \{r, z\}. \quad (12)$$

Equation (12) is weighted by a semi-positive definite matrix, Q_δ . The corresponding term in (10) enables the cell to age more homogeneously as temperature hotspots within the cell are minimised. Moreover, temperature stress and strain in any spatial direction will be reduced. The third term

$$\Delta u_{dc,\varphi}(k+i) = u_{dc,\varphi}(k+1+i) - u_{dc,\varphi}(k+i), \quad (13)$$

is the rate of change of control effort, penalised by a positive definite matrix R . This term limits rapid changes in the duty cycle, reducing switching losses and electrical stress on the components of the ISBC system, thereby prolonging the system's lifetime. Smoothing the control effort helps avoid excessive wear and tear on the power converters. The objective in (10) is subject to the following constraints:

For $i = 0, 1, \dots, N-1$,

$$X(k+1+i) = \bar{A}_d X(k+i) + \bar{B}_d \bar{u}(k+i) + \bar{F}_d w(k+i) \quad (14a)$$

$$Y(k+i) = CX(k+i) + \hat{T}_p(k+i) \quad (14b)$$

$$X(k) = X(0) \quad (14c)$$

$$|T_c(k+i)| \leq T_{c,\max} \quad (14d)$$

$$|u_\varphi(k+i)| \leq u_{\varphi,\max} \quad (14e)$$

$$|u_{dc,\varphi}(k+i)| \leq u_{dc,\varphi,\max}, \quad (14f)$$

where (14a) and (14b) are the discretised versions of the system model (1), (14c) denotes the initial condition, while the remaining constraints (14d)–(14f) denote the box constraints on the system variables, namely the core temperature T_c , the cooling power, and duty cycles, respectively. By restricting T_c , the risk of exceeding the critical temperature that could trigger thermal runaway is minimised. Similarly, limiting u_φ ensures that the cooling power stays within the pump's capacity or maximum allowable coolant flow, while constraining $u_{dc,\varphi}$ keeps the duty cycle within its feasible operation, between 0 and 1.

V. CONTROL SCHEME EVALUATION

A. Benchmarks

The effectiveness of the proposed optimal coolant split scheme is evaluated against two state-of-the-art cooling methods commonly employed in EVs. Typically, cylindrical battery cells are cooled either along their lateral surface (side) only or from the base only, but rarely are both approaches used simultaneously [12,13]. These two conventional cooling schemes, denoted here as side-only cooling and base-only cooling serve as benchmarks for comparison with our optimal scheme, denoted as proposed MPC. The schemes are evaluated across the following key thermal performance metrics; maximum temperature T_{\max} , mean temperature T_{mean} , maximum thermal gradients δT_{\max} , and temperature difference $\Delta T = T_{\max} - T_{\min}$.

Our scheme and its benchmarks can be characterized by their active control inputs. In the proposed MPC, all three control inputs in (7) are actively controlled by the MPC. For side-only cooling, the controller actuates only \bar{u}_s , while both \bar{u}_t and \bar{u}_b remain inactive. In contrast, only \bar{u}_b is active, with the other inputs inactive for base-only cooling.

B. Specification and simulation setup

To demonstrate the scheme for cylindrical cells, we select a large format lithium-iron-phosphate (LFP) 45 Ah cell with specifications similar to those in [5,6]. Without losing generality, the volumetric heat generation rate $q(t)$ is given by a simplified heat generation model [14],

$$q = I(V - V_{ocv})/v_b, \quad (15)$$

where I , V , V_{ocv} , and v_b represent the load current, terminal voltage, open-circuit voltage, and cell volume, respectively. Here, the trajectories of I and V depend on the battery

usage. For this study, we utilize the urban dynamometer driving schedule (UDDS) [15] and scale it by a factor of two to obtain the corresponding heat generation profile, which is shown in Fig. 4a. The UDDS represents city driving conditions for light-duty vehicles. As discussed in Section III-A, q is considered a disturbance in (1). Therefore, the MPC is designed to satisfy the objective in (10) even in the presence of this disturbance.

The MPC simulations are conducted on a MacBook Pro with a 2.6GHz 6-core Intel Core i7 processor and 16GB RAM. The optimization problem is modelled with Yalmip [16] in MATLAB R2023b and solved with Gurobi [17]. The MPC sampling time is set to 1s, with a prediction horizon of 10s. For simplicity, the number of model states in the radial r and axial z directions of the cylindrical cell are chosen to be equal. Specifically, the predictive model consists of four states, with two states for each direction, while the plant model includes 100 states.

In the simulation-based comparison between the proposed MPC with its benchmarks, the initial cell temperatures, $T(r, z, t = 0)$, and the fluid stream temperature T_∞ are set to 15 °C. In [5], a total cooling power of 18 kWm⁻² was equally distributed amongst the three channels, with each channel receiving 6 kWm⁻². In this study, the same total cooling power is used, but the MPC optimally determines the coolant split between the channels to meet the thermal performance objectives. For the objective function, we assign equal importance to all performance metrics by setting the trade-off weights, g_1, g_2 , and g_3 to unity. Additionally, the core temperature is constrained to $0 \leq T_c \leq 40$, and the duty cycle to $0 \leq u_{dc,\varphi} \leq 1$.

C. Results and discussions

Results of the proposed MPC against its benchmarks are shown in Figs. 4 and 5. The proposed MPC demonstrates superior thermal performance in all the considered performance merits. The proposed MPC reduces T_{mean} to about 16 °C, in contrast to about 19 °C for side-only cooling and 23 °C for base-only cooling at the end of the drive cycle. Regarding the thermal gradients, our proposed MPC reduces δT_{max} to about 3 °C/m compared to 6.5 °C/m for side-only cooling and from 5 °C/m for base-only cooling. Similar improvements are observed for T_{max} and the ΔT . Table I summarises the results of the proposed scheme and the benchmarks at the end of the drive cycle.

Side-only cooling outperforms its base-only counterpart in reducing both T_{mean} and T_{max} due to the larger contact area available for heat dissipation on the lateral surface of the cell. Conversely, base-only cooling is more effective at minimizing δT_{max} because it allows for simultaneous cooling of all the rolled electrode layers in the cylindrical cell, resulting in a more homogeneous cooling effect. Our proposed MPC successfully balances these conflicting performance metrics, combining the benefits of both cooling approaches to enhance the overall thermal performance of the battery

cell. The applied average cooling power \bar{u}_φ , as depicted in Fig 5 are optimally distributed across the different sides of the cell under the proposed MPC. In contrast, side-only and base-only cooling apply the maximum cooling power to a single side, i.e., the surface or base, respectively. Moreover, the proposed MPC respects the cooling power limits of $[0, 18]$ kWm⁻², ensuring its practical applicability in real-world cooling. The proposed MPC iterations are solved in 1.02s on average.

TABLE I: Thermal performance merits of three scenarios.

Cooling schemes	T_{max}	T_{mean}	δT_{max}	ΔT
Proposed MPC	17.5	16.0	3.0	5.7
Side-only	22.0	19.0	6.5	10.2
Base-only	25.0	23.0	5.0	11.0

VI. CONCLUSION

This work has presented a model predictive control (MPC) framework for the optimal cooling of cylindrical cells. The proposed MPC harnesses the unique strengths of tab and surface cooling methods to enhance the overall thermal performance of the cell. In addition, the switching mechanism of the power converter was modelled and incorporated into the predictive model to enable us to obtain insights into the optimal coolant distribution to the sides of the cell. The proposed MPC evaluated against conventional side-only and base-only electric vehicle (EV) battery cooling methods under a real-world vehicle driving condition demonstrates superior thermal performance by effectively minimising both the average temperature rise and thermal gradients within the cell. This optimised cooling approach holds significant potential for EVs and battery applications. By maintaining lower and more uniform temperatures across the battery, it effectively slows down degradation processes and potential thermal runaway hazards, ensuring safer battery operation.

REFERENCES

- [1] T. Horiba, T. Maeshima, T. Matsumura, M. Koseki, J. Arai, and Y. Muranaka, "Applications of high power density lithium ion batteries," *J. Power Sources*, vol. 146, no. 1-2, pp. 107–110, 2005.
- [2] C. Bibin, M. Vijayaram, V. Suriya, R. S. Ganesh, and S. Soundarraj, "A review on thermal issues in li-ion battery and recent advancements in battery thermal management system," *Materials Today: Proceedings*, vol. 33, pp. 116–128, 2020.
- [3] C. Bolsinger and K. P. Birke, "Effect of different cooling configurations on thermal gradients inside cylindrical battery cells," *J. Energy Storage*, vol. 21, pp. 222–230, 2019.
- [4] S. Li *et al.*, "Optimal cell tab design and cooling strategy for cylindrical lithium-ion batteries," *J. Power Sources*, vol. 492, p. 229594, 2021.
- [5] G. K. Peprah, Y. Huang, T. Wik, F. Altaf, and C. Zou, "Thermal modelling of battery cells for optimal tab and surface cooling control," *arXiv preprint arXiv:2409.08974*, 2024.
- [6] G. K. Peprah, T. Wik, Y. Huang, F. Altaf, and C. Zou, "Control-oriented 2D thermal modelling of cylindrical battery cells for optimal tab and surface cooling," in *2024 IEEE American Control Conf. (ACC)*, pp. 4651–4656.
- [7] J. Shen, T. Tang, and L.-L. Wang, *Spectral methods: algorithms, analysis and applications*. Springer Science & Business Media, 2011, vol. 41.

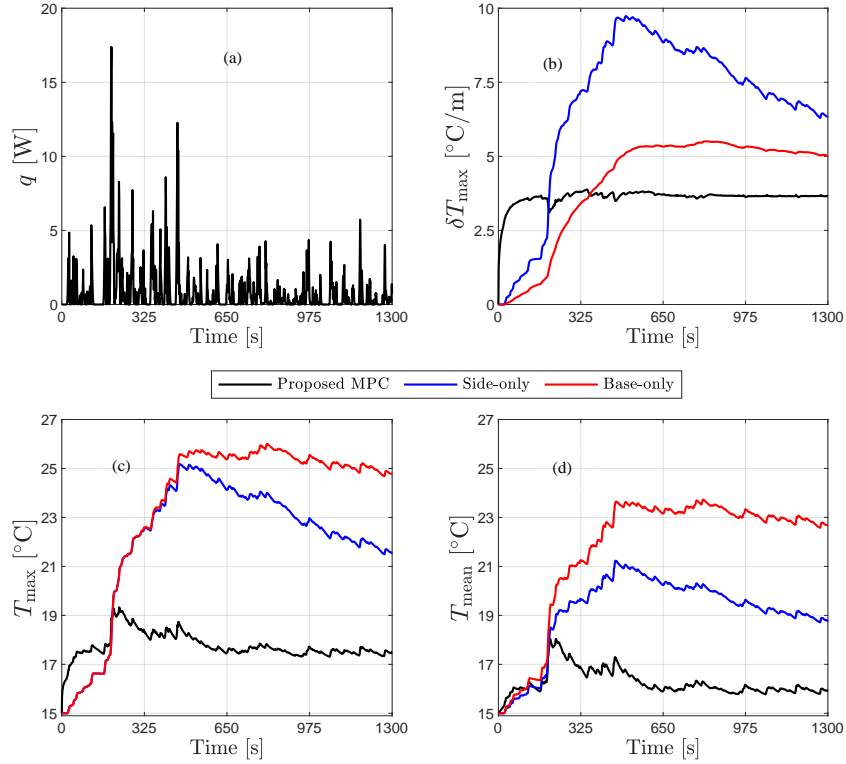


Fig. 4: Comparison of the proposed MPC with side-only and base-only cooling under the UDDS. (a) Heat generation profile of the UDDS. (b) Maximum thermal gradients, δT_{\max} . (c) Maximum temperature, T_{\max} . (d) Mean temperature, T_{mean} .

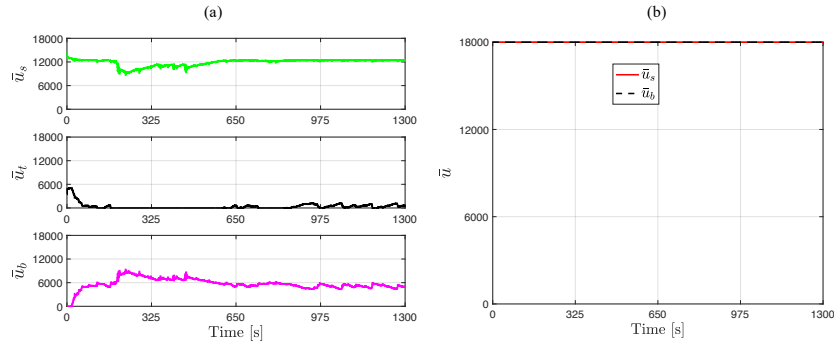


Fig. 5: Evolution of the applied control inputs. (a) Inputs applied by the proposed MPC. (b) Inputs applied by the benchmarks.

[8] M. Taghizadeh, A. Ghaffari, and F. Najafi, "Modeling and identification of a solenoid valve for pwm control applications," *Comptes Rendus Mecanique*, vol. 337, no. 3, pp. 131–140, 2009.

[9] S. V. Angadi and R. L. Jackson, "A critical review on the solenoid valve reliability, performance and remaining useful life including its industrial applications," *Eng. Failure Analysis*, vol. 136, p. 106231, 2022.

[10] G. K. Peprah, F. Liberati, F. Altaf, G. Osei-Dadzie, A. Di Giorgio, and A. Pietrabissa, "Optimal load sharing in reconfigurable battery systems using an improved model predictive control method," in *2021 29th IEEE Mediterranean Conf. on Control and Automation (MED)*, pp. 979–984.

[11] T. Glad and L. Ljung, *Control theory*. CRC press, 2018.

[12] P. R. Tete, M. M. Gupta, and S. S. Joshi, "Developments in battery thermal management systems for electric vehicles: A technical review," *J. Energy Storage*, vol. 35, p. 102255, 2021.

[13] Q. Wang, B. Jiang, B. Li, and Y. Yan, "A critical review of thermal management models and solutions of lithium-ion batteries for the development of pure electric vehicles," *Renewable and Sustainable Energy Rev.*, vol. 64, pp. 106–128, 2016.

[14] D. Bernardi, E. Pawlikowski, and J. Newman, "A general energy balance for battery systems," *J. Electrochem. Soc.*, vol. 132, no. 1, p. 5, 1985.

[15] L. Almatrafi, S. Badaam, and S. M. Qaisar, "Electric vehicle performance evaluation using UDDS, NYCC and WLTP drive cycles," in *2023 20th IEEE Learning and Technology Conf. (L&T)*, pp. 103–108.

[16] J. Lofberg, "Yalmip: A toolbox for modeling and optimization in matlab," in *2004 IEEE Int. Conf. on Robotics and Automation (IEEE Cat. No. 04CH37508)*, pp. 284–289.

[17] B. Meindl and M. Templ, "Analysis of commercial and free and open source solvers for linear optimization problems," *Eurostat and Statistics Netherlands within the project ESSnet on common tools and harmonised methodology for SDC in the ESS*, vol. 20, p. 64, 2012.